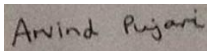


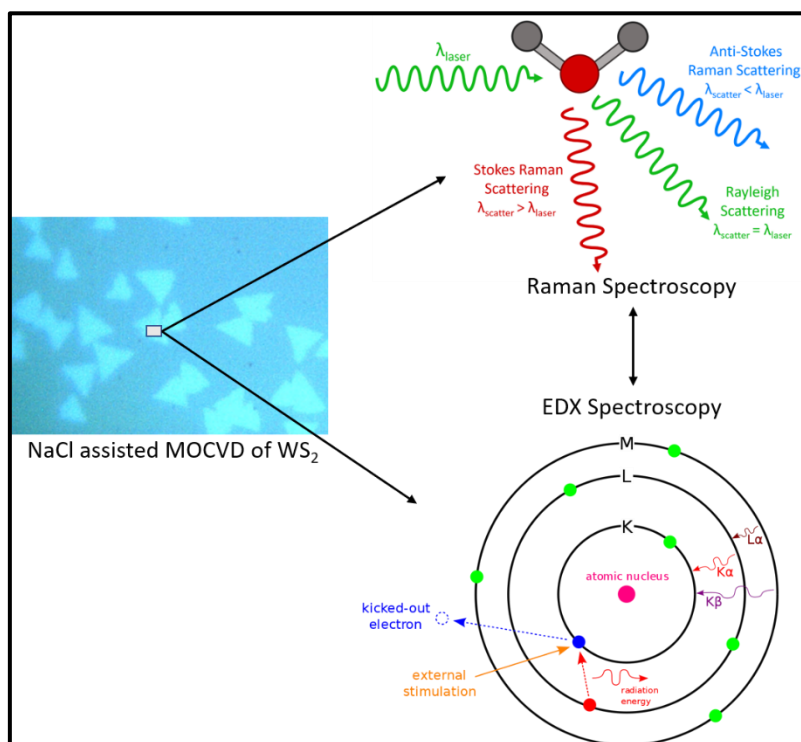
# Characterization of 2D WS<sub>2</sub> grown by NaCl assisted MOCVD

- Arvind Pujari, NanoDTC (c2020)

**Declaration:** “This report is substantially my own work and conforms to the University of Cambridge’s guidelines on plagiarism. Where reference has been made to other research this is acknowledged in the text and bibliography.” 

## Abstract

There has been a great deal of interest in synthesizing large area WS<sub>2</sub> crystals for optoelectronic applications. Metalorganic Chemical Vapour Deposition (MOCVD) has emerged as a scalable method for this, however, there are still significant differences in terms of crystallinity and optical properties even when synthesis is carried out under the same conditions. Using NaCl as a growth promoter in MOCVD has emerged as a technique to obtain large area crystals with consistent optical and electrical properties. In this report, we attempt to correlate the quality of WS<sub>2</sub> crystals (through Raman and PL spectra) with the amount of NaCl used through EDX spectroscopy. The effect of laser power on Raman and PL measurements are also considered. Raman and PL maps are analysed as a way to provide large-area information about the uniformity of the sample.



## 1. Introduction

2D transition metal dichalcogenides have attracted a great deal of attention over recent years because of the existence of a direct band gap, which makes them well suited for a variety of optoelectronic and nanoelectronic applications. In particular, a great deal of attention has been focussed on two-dimensional tungsten disulfide (2D WS<sub>2</sub>) which has a unique band structure leading to broadband spectral response characteristics, ultra-fast bleach recovery time and excellent saturable light absorption [1].

The structure of one-dimensional WS<sub>2</sub> is shown in Figure 1 and consists of stacked triple layers of a W atom layer sandwiched between two S layers, with all layers having a hexagonal lattice structure. As the adjacent layers are held together by weak Van der Waals forces, peeling of layers to form a single layered structure is possible. This is particularly interesting because when the thickness of WS<sub>2</sub> is reduced to a single layer, the indirect band gap, which lies below the direct gap in the bulk material, shifts upwards in energy by more than 0.6 eV. This leads to a crossover to a direct-gap material in the limit of the single monolayer[2]. Indeed, monolayer WS<sub>2</sub> displays a optical band gap of 2 eV and bright room temperature photoluminescence [3].

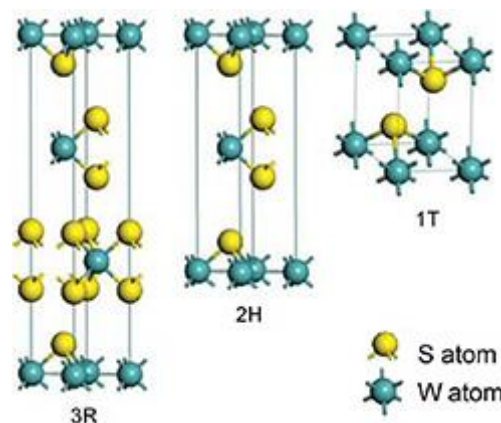


*Figure 1. A WS<sub>2</sub> unit cell consisting of stacked triple layers [4].*

The presence of a direct band gap in the visible regime (620 nm) has led to a large amount of research into growing large area 2D monolayers of WS<sub>2</sub>. The most common methods of 2D WS<sub>2</sub> preparation include pulsed magnetron sputtering, mechanical and liquid phase exfoliation, pulsed laser deposition (PLD) and chemical vapour deposition (CVD). Of these, CVD has been used extensively for the synthesis of monolayer WS<sub>2</sub> [5] [6]. This is done in a quartz tube furnace whilst using an inert gas as a carrier gas for reaction precursors. The precursors typically used are WO<sub>3</sub> and S, [7]. Metalorganic Chemical Vapour Deposition (MOCVD) has also been used to grow large area WS<sub>2</sub> monolayers. Park et. al. [8] used (C<sub>2</sub>H<sub>5</sub>)<sub>2</sub>S, Mo(CO)<sub>6</sub>

and  $W(CO)_6$  precursors to synthesize 2D  $WS_2$  with spatially uniform high carrier mobility ( $\mu_{FE}$  as high as  $18 \text{ cm}^2 \text{ V}^{-1} \text{ s}^{-1}$  at room temperature and a median  $\mu_{FE}$  close to  $5 \text{ cm}^2 \text{ V}^{-1} \text{ s}^{-1}$ ). However, the dimension, crystallinity, optical properties, and morphology of 2D  $WS_2$  monolayers synthesized by CVD varies dramatically even under the same growth conditions [9]. High temperatures (or low pressures) are needed to increase the mass flux of gaseous tungsten species in the reaction chambers which increases powers costs and introduces thermal strain between the  $WS_2$  crystals and substrate [10].

As an alternative, to reduce the temperatures and promote growth, halide salts such as NaCl are used as a promoters since they can react with  $WO_3$  to form volatile oxhalide intermediates such as  $WO_xCl_y$ . These intermediates can react with sulphur gas at a temperature of 700-850 °C and facilitate  $WS_2$  nucleation leading to large area, high quality  $WS_2$  monolayers.

There have been few reports correlating the concentration of NaCl with the size and quality (via Raman and PL spectra) of  $WS_2$  crystals grown via NaCl assisted MOCVD. In this project, 2D  $WS_2$  was grown on sapphire ( $Al_2O_3$ ) substrates using NaCl assisted MOCVD. Optical characterization of two-dimensional  $WS_2$  was carried out using Raman spectroscopy while chemical compositions were determined using EDX.

## 2. Methods

### 2.1 NaCl assisted synthesis of 2D $WS_2$

Samples were provided by the Hofmann group. 1cm by 1cm sapphire chips (Alfa Aesar, c-plane  $\pm 0.3^\circ$ , single side polished) were used as growth substrates. MOCVD growth was carried out in a custom-made cold-wall low pressure laser-CVD system. An 808 nm continuous wave (CW) IR laser with a maximum power of 60 W is used for remote sample heating. In order to achieve a homogeneous beam profile, a beam shaper is used to create a top-hat (instead of Gaussian) profile at the focal point, which has a size of  $5 \text{ mm} \times 5 \text{ mm}$ . Due to very localized heating, the sample was placed (as received) on a graphite susceptor to increase the temperature heating uniformity and loaded in the MOCVD chamber. Sample temperature was monitored by a  $1.6 \mu\text{m}$  IR pyrometer, with the setting of transmission = 0.9 and emissivity = 0.9. Before growth, the chamber was pumped down to  $<10^{-2}$  millibar, and then filled to 80mbars by Ar. The growth has been carried by co-exposing the sample to a mixture of  $W(CO)_6$  (Strem Chemicals, 99.9%+ purity),  $(CH_3)_2S_2$  (Sigma Aldrich, 99%+ purity) gases and  $H_2O$  (DI water) vapor. Here,

the H<sub>2</sub>O was used to remove carbon deposition, as previously reported [11]. The flows of all precursors were controlled by leak valve. Giving the relatively low vapour pressure (0.13 mbar at 20°C), and thus slow evaporation rate, of THC at room temperature, 5 sccm of Ar was passed through the THC bubbler as carrier gas. Meanwhile, the H<sub>2</sub>O tank was heated to 40 °C to provide enough vapour pressure.

During the reaction, the 3 leak valves controlling the flow of THC, DMDS and H<sub>2</sub>O were opened 8 turns, 8 turns and 5 turns, respectively. After the pressure has been stabilized at 80 millibars, the growth was initiated by rapidly heating the sample to 900 °C. The ramp rate was estimated at around 40C/s. The temperature measurement error was estimated as ~50 °C. Each growth duration was kept at 15 minutes. After growth, the laser was turned off, the THC and H<sub>2</sub>O valves were closed, and the sample was cooled in a sulfur rich atmosphere to impede sulfur vacancies forming.

For those samples with NaCl as growth promoter, some pre-treatment was done. Specifically, before the growth, the sapphire substrate was pre-annealed in 80 millibars Ar/H<sub>2</sub>O (8 turns H<sub>2</sub>O leak valve) at 900 °C for 10 minutes to remove surface carbon and organic contamination and improve hydrophilicity. Then, a solution of 200 mg NaCl dissolved in 100mL DI water was drop-casted onto the sapphire sample and let dry on a hot plate at 40 °C. Then, the sample was loaded in the MOCVD chamber and growth was proceeded as above.

## *2.2 Raman and PL Spectroscopy*

Raman spectroscopy was carried out by a Reinshaw inVia confocal Raman microscope. The wavelength of the excitation laser was set at 535 nm. Laser power was varied between 1% and 50%. For Raman measurements, the acquisition time was set at 1s, with 1 acquisition taken, whilst for the PL measurements, acquisition time was set at 10s, with one acquisition taken.

2D transition metal chalcogenides typically have four Raman modes: A<sup>1</sup><sub>g</sub>, E<sup>1</sup><sub>g</sub>, E<sup>1</sup><sub>2g</sub> and E<sup>2</sup><sub>2g</sub>. However, the E<sup>1</sup><sub>g</sub> mode and low energy E<sup>2</sup><sub>2g</sub> mode are typically absent in measurements due to the forbidden selection rule in the back-scattering geometry and the limited rejection against Rayleigh scattering respectively [12]. The typical out-of-plane A<sup>1</sup><sub>g</sub> and in-plane E<sup>1</sup><sub>2g</sub> modes are seen in Figure 2, located at 420 cm<sup>-1</sup> and 350 cm<sup>-1</sup> respectively. We measure the distance between the E<sup>1</sup><sub>2g</sub> and A<sup>1</sup><sub>g</sub> modes – this is typically indicative of the number of layers present in the sample (Figure 2), and the ratio between the heights of the E<sup>1</sup><sub>2g</sub> and A<sup>1</sup><sub>g</sub> modes.

The  $E_{2g}^1$  mode typically shows little dependence on the film thickness while the  $A_{1g}^1$  mode undergoes a blue shift with an increasing number of layers due to a lattice stiffening effect when different layer thicknesses are added [12].

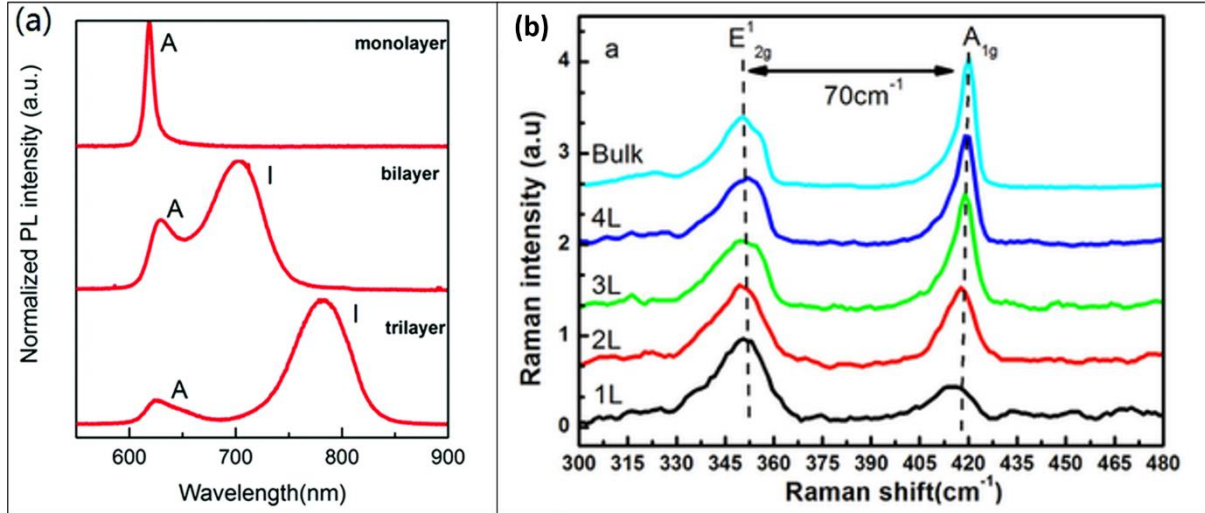


Figure 2. Typical Raman and PL spectra of atomically thin  $WS_2$  [12], [13].

### 2.3 EDX Spectroscopy

EDX data was obtained using a Helios NanoLab 600 microscope. The acceleration voltage was varied between 5 and 20 KeV. The beam current was 5 nA. The electron beam was perpendicular to the surface of the sample. An Everhart-Thornley detector was used to detect secondary electrons whilst a Silicon Drift Detector (Oxford Instruments) was used for X-Ray (EDX) detection.

## 3. Results

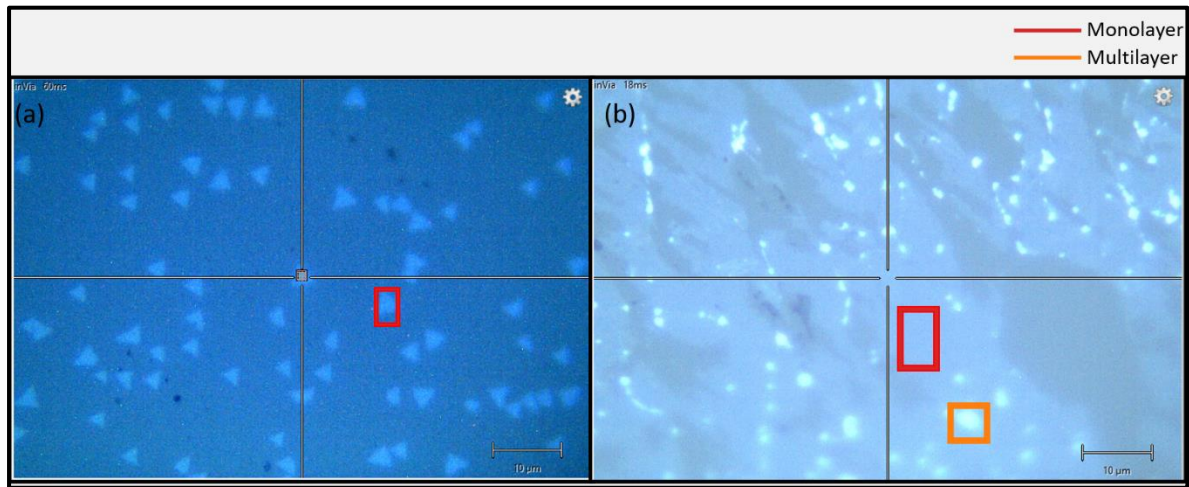


Figure 3. Optical microscopy images (under 100x zoom) of  $WS_2$  samples grown on sapphire (a) without NaCl and (b) with NaCl. Triangular domains are seen in the sample grown without

*NaCl whereas continuous domains are seen in the region grown with NaCl. Red and orange boxes indicate monolayer and multilayer regions, respectively.*

Optical microscopy images of WS<sub>2</sub> grown using MOCVD on sapphire with and without NaCl are shown in Figure 1 (a) and (b) respectively. The bright triangular regions are WS<sub>2</sub> domains. The brightest regions in Figure 1(b) correspond to regions where the number of layers is higher. Thus, it is evident that NaCl assisted MOCVD can be used to grow large area WS<sub>2</sub> domains.

### *3.1 Raman Spectra of WS<sub>2</sub> samples grown on sapphire without NaCl*

Figure 4 shows the Raman spectra of WS<sub>2</sub> grown on sapphire using MOCVD (without NaCl) for a variety of laser powers. The spectra are normalized for different laser powers. The E<sub>2g</sub><sup>1</sup> mode is seen at 353.9 cm<sup>-1</sup> while the A<sub>g</sub><sup>1</sup> mode is seen at 418 cm<sup>-1</sup> (difference of 64 cm<sup>-1</sup>) which is consistent with reported values in literature [12]. The peak at 324 cm<sup>-1</sup> has been reported for monolayer WS<sub>2</sub> [14], indicating the region is monolayered. The peaks seen at 578 and 645 cm<sup>-1</sup> are similar to the values of the Raman spectra of sapphire reported in literature [15]. It is interesting to note that the peak intensities of the E<sub>2g</sub><sup>1</sup> and A<sub>g</sub><sup>1</sup> modes, and their relative intensities change with changing laser power. Figure 4(a) shows the Raman spectra of the sample (normalized by laser power) as the laser power is decreased from 50% to 5% and then 1%: the run with 1% laser power has a much stronger signal than the run with 5% and 50% power. Another unusual trend is seen in Figure 4(b) when the laser power is gradually increased from 1% to 50% and then decreased back to 1%: a stronger signal is obtained when 10% power is used vs. 50%, however when 10% power is used again the signal rapidly drops. There is no observed correlation between the laser power and peak intensities of the normalized Raman spectra. It is important to note this effect and take several measurements at different laser powers while comparing the spectra of two different samples.

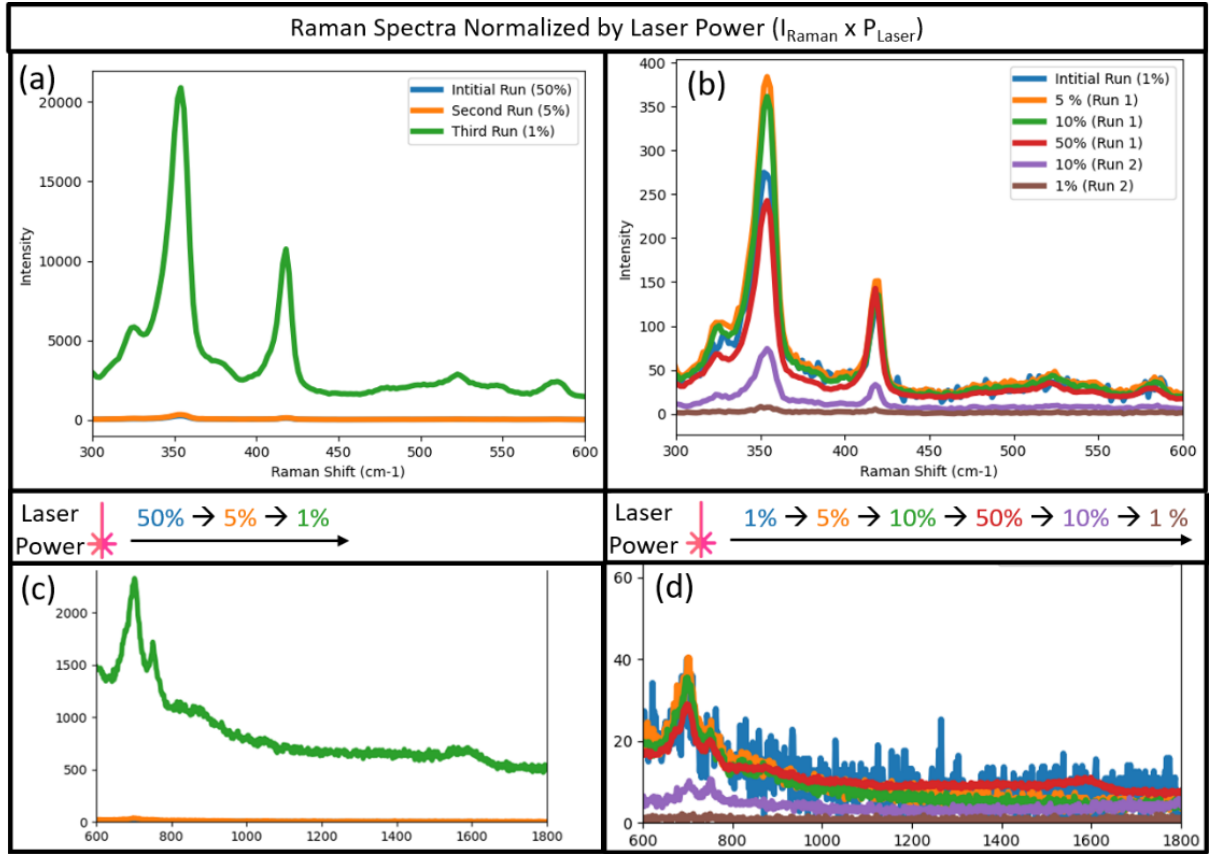


Figure 4. The Raman Spectra of a WS<sub>2</sub> crystal grown on sapphire (without NaCl) as the laser power is (a) decreased from 50% to 1% (b) increased from 1% to 50% and then decreased to 1%. Raman spectra between 600 and 1500 cm<sup>-1</sup> of figures (a) and (b) are shown in (c) and (d) respectively. The arrows in the figure indicate the sequence of laser powers used.

Figure 4(c) and (d) indicate that there is no amorphous carbon present in the sample as seen by the absence of a peak at 1518 cm<sup>-1</sup> [16].

This effect is further illustrated in Figure 5 which shows the peak ratios ( $R = E_{2g}^1 / A_{1g}^1$ ) for a variety of laser powers. It is interesting to note that at the same spot, when different laser powers are used, the value of  $R$  changes from a value of 1.9 when 1% laser power is initially used, to a value of 1.4 when the laser power is increased and decreased back to 1%. As illustrated before, the value of  $R$  is important for determining the number of layers present in the sample. The position of the peaks and the difference between them is largely consistent (some anomalies exist, mean peak distance = 64.85 cm<sup>-1</sup>, median peak distance = 64.0 cm<sup>-1</sup>, SD = 4.82 cm<sup>-1</sup>) which indicate that the laser power does not affect the peak positions.

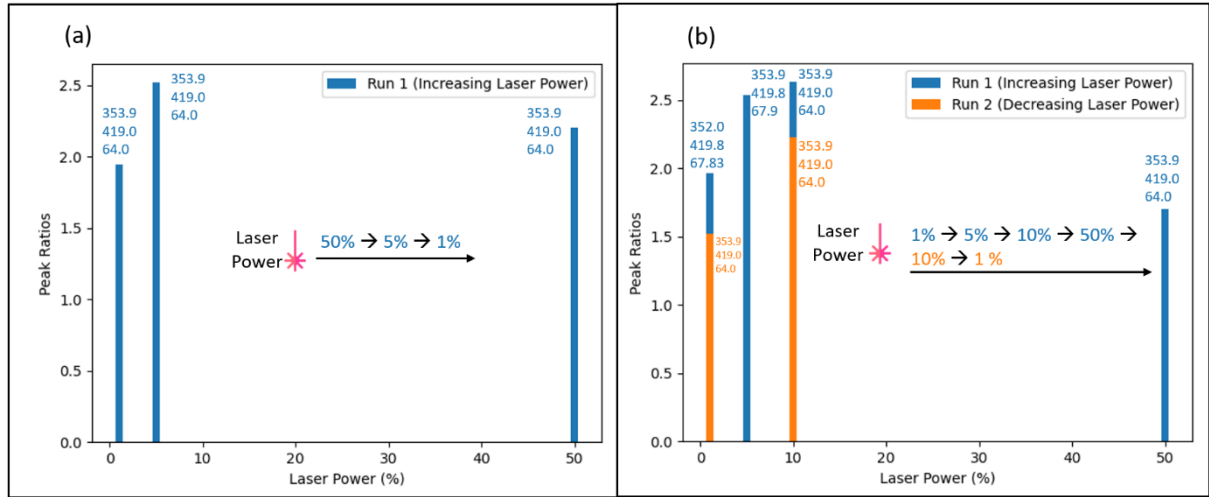


Figure 5. The effect of laser intensity on the peak ratio ( $R$ ) of the Raman spectra of a  $WS_2$  sample for two different sequences of laser power. The value in the brackets are the positions of the  $E_{2g}^I$ ,  $A_g^I$  and their difference ( $cm^{-1}$ ), respectively. The sequence of laser power is the same as in Figure 4. When the laser power is increased from 1% and decreased back to 1%, the value of  $R$  changes from 2 to 1.5.

### 3.2 PL Spectra of $WS_2$ samples grown on sapphire without NaCl

The PL spectra of the same spots on the sample are shown in Figure 6, with varying laser intensities used. The PL spectra are normalized with respect to the laser power. A variation in the area under the curve and the peak position of the PL spectra are also seen. Upon starting from a laser power of 1%, increasing the laser power and then decreasing it back to 1%, the strongest spectra is obtained from the final run. The peak of the spectra varies from 1.85 to 1.96 (lower than the reported value of 2.01 eV [17] for a monolayer). This shift could be the result of tensile strain in the sample since strain can change the positions of the minimums of the conduction and valence band. For example Pak et al [18] showed that an applied strain of 0.6% can move the PL peak of monolayer  $WS_2$  from 2.02 to 1.98. A strong PL is seen at an energy of 1.80 eV. This is the characteristic PL spectra of sapphire and originates due to trace amounts of  $Cr^{3+}$  in the substrate [19] [20]. The bumps seen in the 1% laser power spectra may originate from defect-bound exciton emission [21].



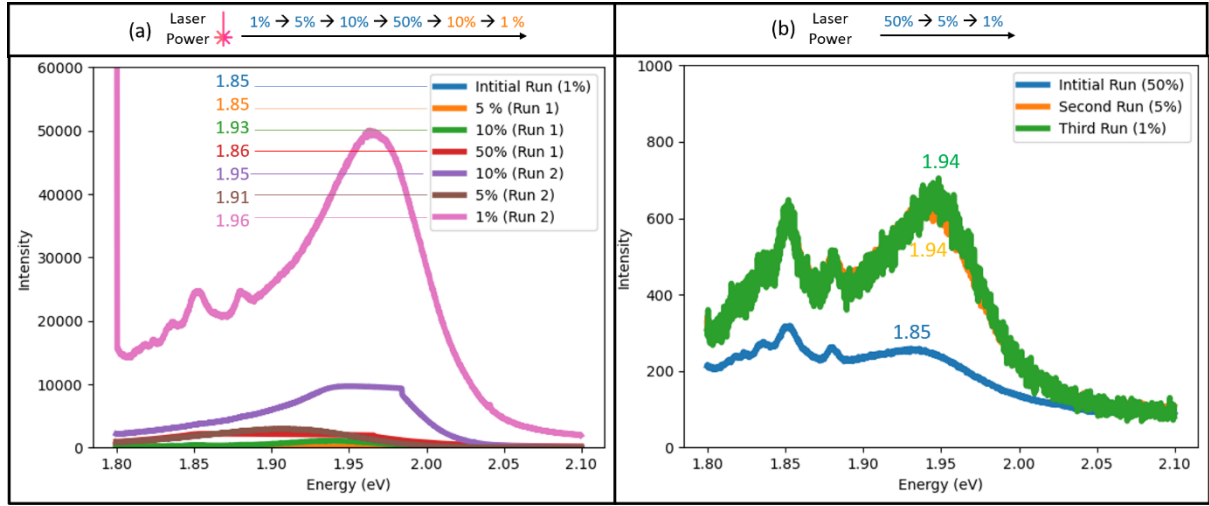


Figure 6. The PL spectra (normalized by laser power) of WS<sub>2</sub> grown on sapphire with the same sequence of laser powers as Figure 4. A variation in PL intensity is seen with laser power. The position of the peaks are indicated in the figure.

The variations in PL and Raman spectra with varying laser power has been reported before [22]. Some of the reasons which may lead to this include quenching by amorphous carbon present on the sample: this would provide a pathway for excitons and holes to separate, preventing their radiative recombination and decreasing the observed PL intensity. However, as can be seen in the Raman spectra of our sample, there is no indication of amorphous carbon being present. Laser annealing has also been reported to affect PL spectra since there is a significant decrease in the photoluminescence generated from dislocation-induced defects and an increase in band-to-band emission [23]. It has also been reported that weak PL is a consequence of the formation of trions (negatively charged excitons) and the switch from trion to exciton emission (via annealing or molecular adsorption) can dramatically increase the PL [24] which may be the case here.

### 3.2 Raman and PL Spectra of WS<sub>2</sub> samples grown on sapphire with NaCl

The Raman and PL spectra of a WS<sub>2</sub> sample grown on sapphire by NaCl assisted MOCVD can be seen in Figure 7. The ratio between the heights of the E<sub>2g</sub><sup>1</sup> and A<sub>g</sub><sup>1</sup> modes is 6.06 and 5.80 for 1% and 0.5% laser power respectively. Although the Raman spectra at both laser powers show good agreement, there is not enough data to comment about whether a similar photo annealing effect is observed with this sample. The peak of the PL spectra is at 2 eV, which is consistent with literature values [17]. The Raman spectra between 600 and 1800 cm<sup>-1</sup> shows no peaks corresponding to amorphous carbon.

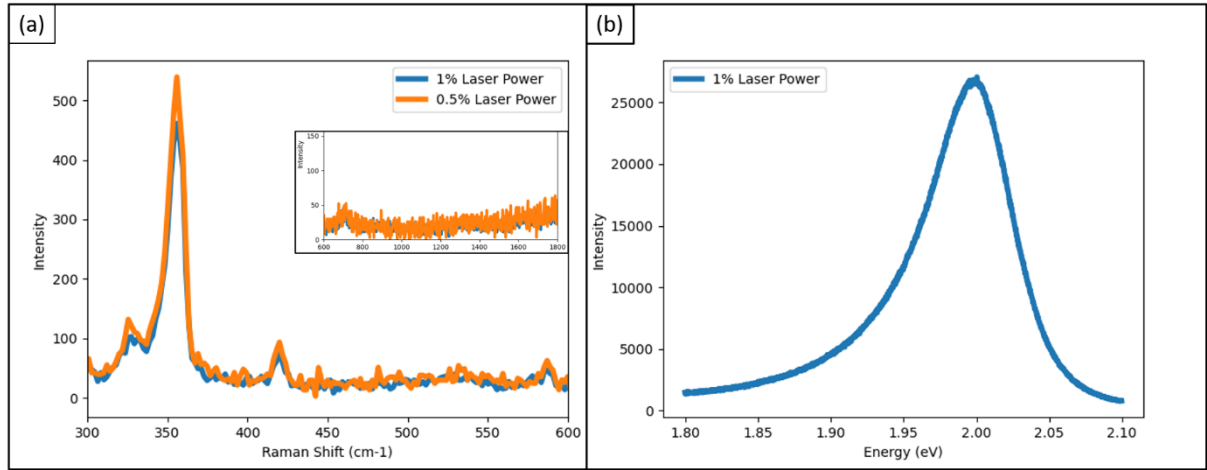


Figure 7. Normalized Raman (a) and PL (b) spectra of  $\text{WS}_2$  grown on sapphire by NaCl assisted MOCVD. A strong PL is observed, with a peak at 2 eV. Inset figure is Raman spectra between 600 and 1800  $\text{cm}^{-1}$ .

### 3.3 Peak Deconvolution

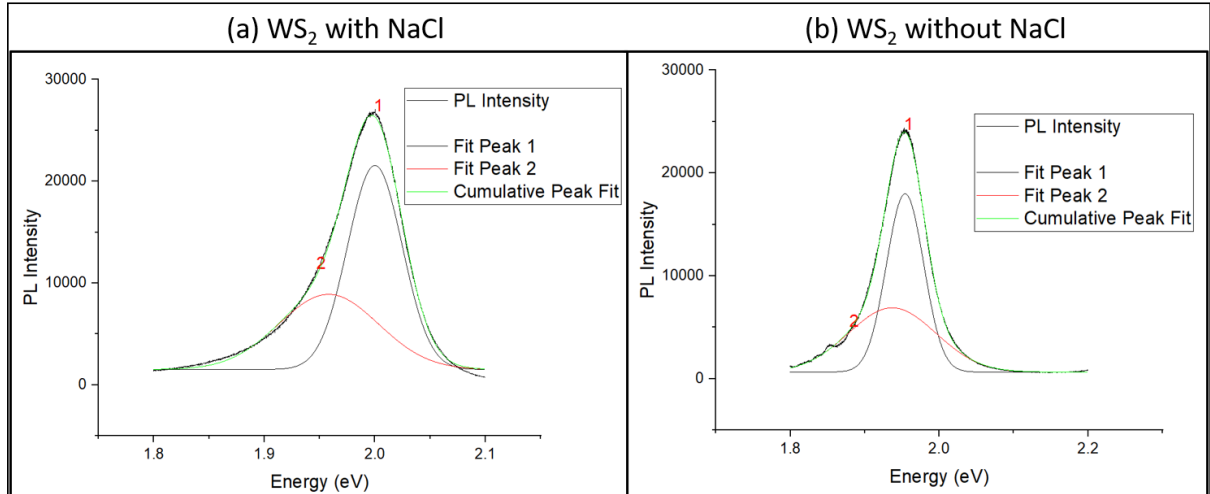


Figure 8. Peak deconvolution of PL spectra of a  $\text{WS}_2$  sample (a) synthesized by NaCl assisted MOCVD and (b) without NaCl. The red lines are the contributions from the trion while the black lines are from the exciton.

Peak deconvolution of the PL spectra was carried out using OriginLab and can be seen in Figure 8. The red line corresponds to the trion peak and the black line to the exciton peak. The relative contributions of the exciton and trion peaks to the overall sample remain roughly equal.

### 3.4 Raman and PL Maps

In order to study the spatial variation in Raman and PL, a raster scan across a 6x6 grid was carried out. The results for the  $\text{WS}_2$  sample prepared with and without NaCl are shown in Figure 9. While a comparison of the map data will not be accurate since Figure 9 (a)-(d)

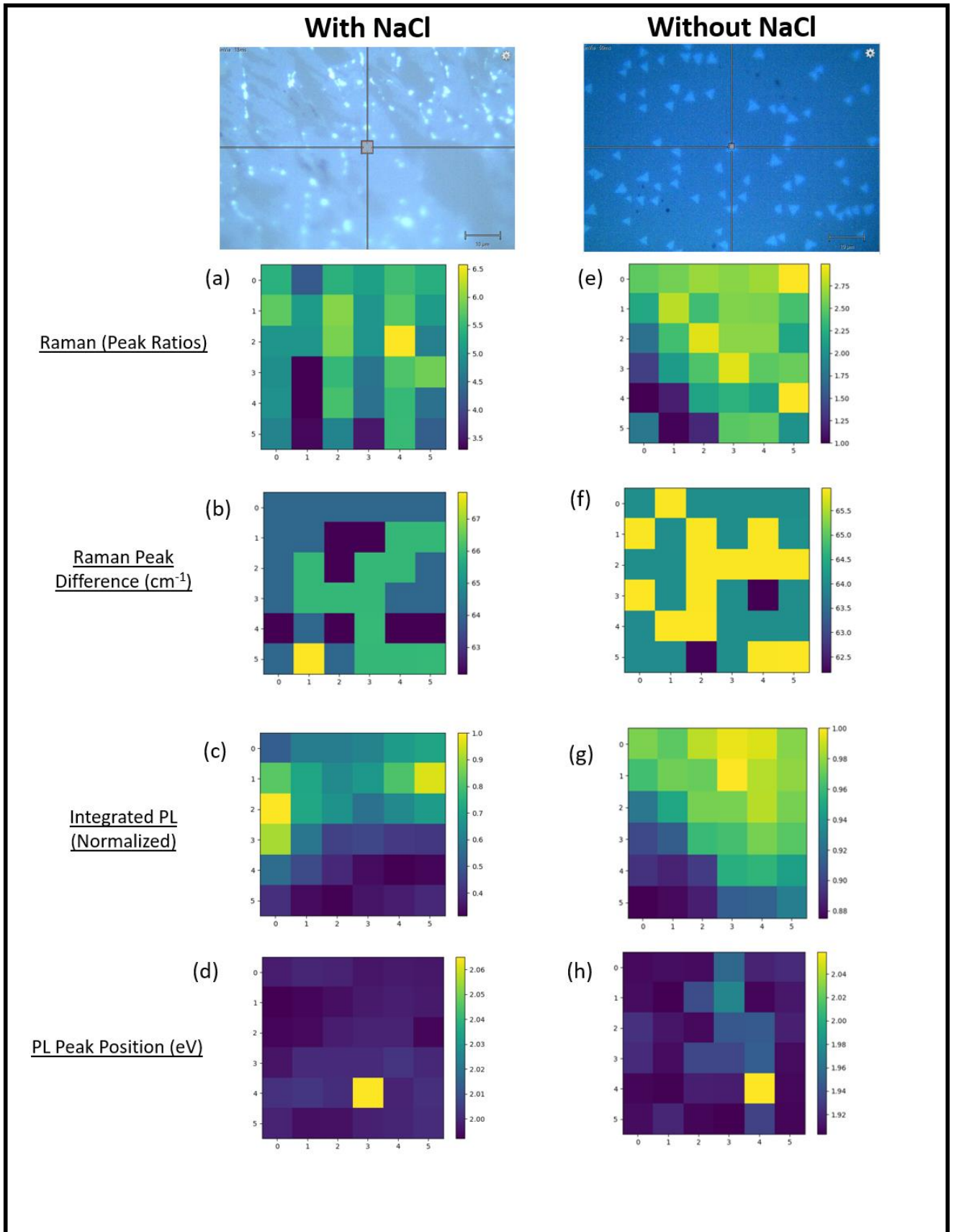


Figure 9. Raman and PL Map data for WS<sub>2</sub> samples grown with and without NaCl.

correspond to a continuous domain while Figure 9 (e)-(f) correspond to a singular triangular domain, other inferences can be made.

The Raman peak ratios across the NaCl sample are of the order of 3-6 while the peak distances are 63-67  $\text{cm}^{-1}$  indicating that this region may be a monolayer. For the sample grown without NaCl, the peak ratios lie between 1 and 2.75 whilst the distance between the peaks is 62.5-65.5  $\text{cm}^{-1}$  indicating that this may be a multi-layered region.

The average position of the PL peak in the sample grown with NaCl is 2.01 eV whilst in the sample grown without NaCl it is 1.92 eV. This is consistent with the red shifting of the main PL peak as the number of layers increases [13].

### 3.5 EDX Data

In order to correlate domain size/quality of  $\text{WS}_2$  with the amount of NaCl used, EDX measurements were carried out. As the  $\text{K}\alpha$  line of W is located at 8.2eV, initially, an acceleration voltage of 20KeV was used (acquisition time of 20 s). However, this failed to detect anything other than Al, O (elements present in the substrate, sapphire) and C due to the small interaction volume of the sample (height of monolayer  $\text{WS}_2$  is approximately 0.6 Å). Hence, the EDX signal was dominated by the substrate. Figure 10 shows Monte Carlo simulations for a simulation geometry of 1nm  $\text{WS}_2$  on a sapphire substrate at 5 and 20 kV. As expected, most of the electron trajectories correspond to the sapphire substrate, making the detection of x-rays from the  $\text{WS}_2$  sample tricky. At a lower acceleration voltage, the beam specimen interaction for the sample is higher.

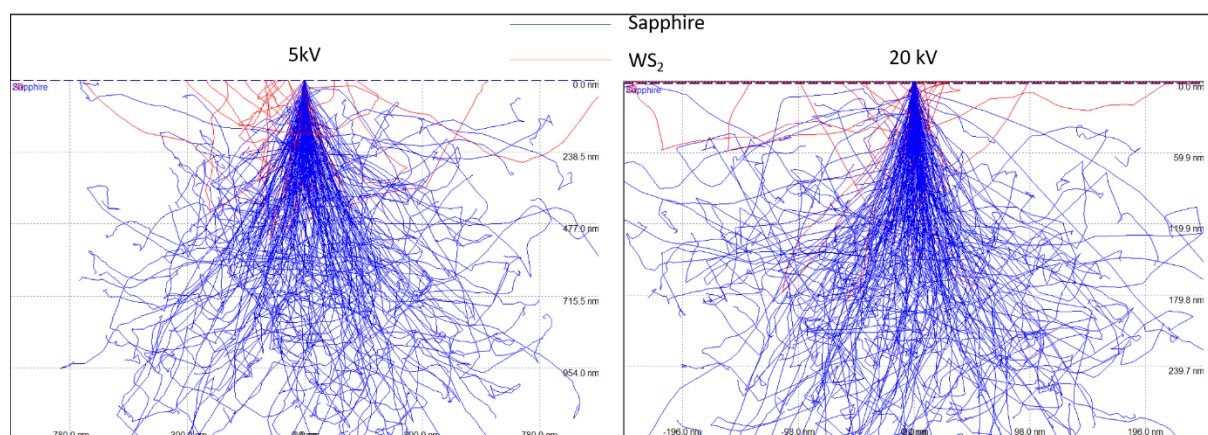


Figure 10. Monte Carlo simulations of beam specimen interactions for a 1nm  $\text{WS}_2$  sample on a sapphire substrate at 5 and 20 kV.

Figure 11 shows the SEM and corresponding EDX images of WS<sub>2</sub> grown on Al<sub>2</sub>O<sub>3</sub> by NaCl assisted MOCVD. At a higher acceleration voltage (20 kV) W and S are not detected. This is probably due to the small interaction volume for the beam. To reduce the dominance of the substrate on the EDX spectra, a lower acceleration voltage was used (5 kV). This comes at the cost of skipping the K $\alpha$  line of W, however the EDX detector was able to detect W and S in the sample. It was less successful at detecting Na and Cl which meant that the EDX data could not be correlate with the Raman and PL data. For the determination of elemental composition of 2D materials, XPS is likely to be a more useful tool than EDX. This is because EDX effectively gives the bulk composition of the sample (due to the nature of electron specimen interactions), while XPS (which relies on generated photoelectrons) gives the near surface chemical composition of the sample (elements present near the top 10nm of the sample).

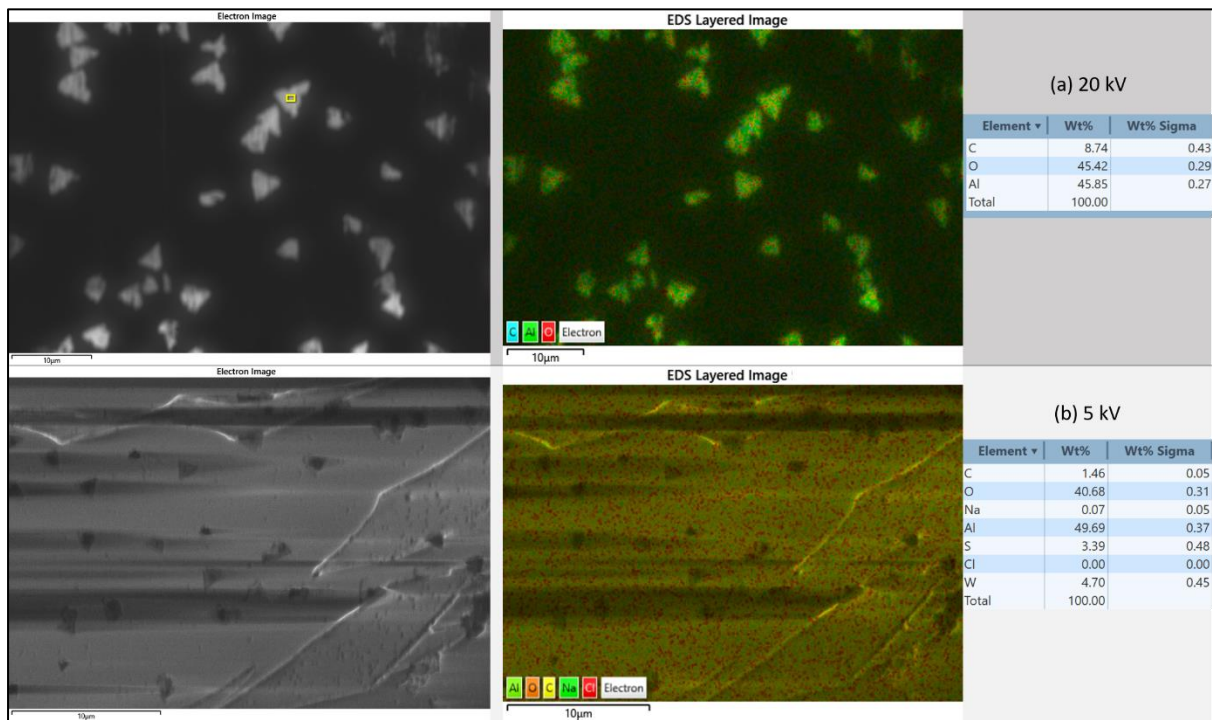


Figure 11. SEM and EDX images of WS<sub>2</sub> grown with NaCl at different acceleration voltages.

#### 4 Conclusion

The initial aim of this work was to correlate Raman and PL spectra of 2D WS<sub>2</sub> grown on sapphire through NaCl assisted MOCVD with the elemental composition of the sample. However, elemental analysis of 2D materials using EDX is tricky due to the small interaction

volume of the beam, which means that the elemental signature is dominated by the substrate. Therefore, XPS may be a better characterization tool for this purpose since its interaction is related to the surface (approximately top 10nm).

It is observed that the Raman and PL spectra vary with the laser power used even after normalization. The ratio and distance between the  $E^1_{2g}$  and  $A^1_g$  modes vary with the laser power applied which is of consequence for measurements. Some of the reasons for this, as reported in literature include laser annealing: due to a decrease in the photoluminescence generated from dislocation-induced defects and an increase in band-to-band emission as well as a change in state from trion to exciton emission.

## 5 Acknowledgements

I would like to thank Ye Fan and Vlad Veigang-Radulescu for taking time out of their busy schedules to supervise this project at extremely short notice and for providing the samples. I would also like to thank Eric Tapley from the Physics microscopy suite for his help with SEM and EDX training.

## 6 References

- [1] J. Ding, A. Feng, X. Li, S. Ding, L. Liu, and W. Ren, "Properties, preparation, and application of tungsten disulfide: a review," *J. Phys. Appl. Phys.*, vol. 54, no. 17, p. 173002, Feb. 2021, doi: 10.1088/1361-6463/abd9e8.
- [2] K. F. Mak, C. Lee, J. Hone, J. Shan, and T. F. Heinz, "Atomically Thin  $\text{MoS}_2$ : A New Direct-Gap Semiconductor," *Phys. Rev. Lett.*, vol. 105, no. 13, p. 136805, Sep. 2010, doi: 10.1103/PhysRevLett.105.136805.
- [3] H. R. Gutiérrez *et al.*, "Extraordinary room-temperature photoluminescence in WS<sub>2</sub> monolayers," p. 25.
- [4] "Full article: Nanoscale Transition Metal Dichalcogenides: Structures, Properties, and Applications."  
[https://www.tandfonline.com/doi/full/10.1080/10408436.2013.863176?casa\\_token=OV3qH3xQRuEAAAAA%3AKyGJS1WSHjfOZ073HVatAMMx2sGBHP1I\\_PgZnvCSX4n4v0VWbrT0o6MgyA9s2C\\_CEL\\_PZYge7w](https://www.tandfonline.com/doi/full/10.1080/10408436.2013.863176?casa_token=OV3qH3xQRuEAAAAA%3AKyGJS1WSHjfOZ073HVatAMMx2sGBHP1I_PgZnvCSX4n4v0VWbrT0o6MgyA9s2C_CEL_PZYge7w) (accessed May 01, 2021).
- [5] "Chemically Driven Tunable Light Emission of Charged and Neutral Excitons in Monolayer WS<sub>2</sub> | ACS Nano."  
[https://pubs.acs.org/doi/abs/10.1021/nn504196n?casa\\_token=6ZBoooIySH8AAAAA:7GxVLCWhir9u0VLk7NvwXgXLtIsQt\\_p1WNa2aNd4OXFJSwlb7pOyh2XRTGhZu8sLPngMldc9rr9](https://pubs.acs.org/doi/abs/10.1021/nn504196n?casa_token=6ZBoooIySH8AAAAA:7GxVLCWhir9u0VLk7NvwXgXLtIsQt_p1WNa2aNd4OXFJSwlb7pOyh2XRTGhZu8sLPngMldc9rr9) (accessed May 01, 2021).
- [6] Z. Y. Zhu, Y. C. Cheng, and U. Schwingenschlögl, "Giant spin-orbit-induced spin splitting in two-dimensional transition-metal dichalcogenide semiconductors," *Phys. Rev. B*, vol. 84, no. 15, p. 153402, Oct. 2011, doi: 10.1103/PhysRevB.84.153402.
- [7] K. M. McCreary, A. T. Hanbicki, G. G. Jernigan, J. C. Culbertson, and B. T. Jonker, "Synthesis of Large-Area WS<sub>2</sub> monolayers with Exceptional Photoluminescence," *Sci. Rep.*, vol. 6, no. 1, Art. no. 1, Jan. 2016, doi: 10.1038/srep19159.



- [8] K. Kang *et al.*, “High-mobility three-atom-thick semiconducting films with wafer-scale homogeneity,” *Nature*, vol. 520, no. 7549, Art. no. 7549, Apr. 2015, doi: 10.1038/nature14417.
- [9] B. Shi *et al.*, “High-efficiency synthesis of large-area monolayer WS<sub>2</sub> crystals on SiO<sub>2</sub>/Si substrate via NaCl-assisted atmospheric pressure chemical vapor deposition,” *Appl. Surf. Sci.*, vol. 533, p. 147479, Dec. 2020, doi: 10.1016/j.apsusc.2020.147479.
- [10] L. Dong *et al.*, “Facile access to shape-controlled growth of WS<sub>2</sub> monolayer via environment-friendly method,” *2D Mater.*, vol. 6, no. 1, p. 015007, Oct. 2018, doi: 10.1088/2053-1583/aae7eb.
- [11] Y. Fan *et al.*, “Understanding metal organic chemical vapour deposition of monolayer WS<sub>2</sub>: the enhancing role of Au substrate for simple organosulfur precursors,” *Nanoscale*, vol. 12, no. 43, pp. 22234–22244, 2020, doi: 10.1039/D0NR06459A.
- [12] H. Zeng *et al.*, “Optical signature of symmetry variations and spin-valley coupling in atomically thin tungsten dichalcogenides,” *Sci. Rep.*, vol. 3, no. 1, Art. no. 1, Apr. 2013, doi: 10.1038/srep01608.
- [13] L. Yuan and L. Huang, “Exciton dynamics and annihilation in WS<sub>2</sub> 2D semiconductors,” *Nanoscale*, vol. 7, no. 16, pp. 7402–7408, Apr. 2015, doi: 10.1039/C5NR00383K.
- [14] A. Berkdemir *et al.*, “Identification of individual and few layers of WS<sub>2</sub> using Raman Spectroscopy,” *Sci. Rep.*, vol. 3, no. 1, Art. no. 1, Apr. 2013, doi: 10.1038/srep01755.
- [15] M. Kadleíková, J. Breza, and M. Veselý, “Raman spectra of synthetic sapphire,” *Microelectron. J.*, vol. 32, no. 12, pp. 955–958, Dec. 2001, doi: 10.1016/S0026-2692(01)00087-8.
- [16] M. Marton *et al.*, “Raman Spectroscopy of Amorphous Carbon Prepared by Pulsed Arc Discharge in Various Gas Mixtures,” *J. Spectrosc.*, vol. 2013, p. e467079, Nov. 2012, doi: 10.1155/2013/467079.
- [17] Y. Kwon, K. Kim, W. Kim, S. Ryu, and H. Cheong, “Variation of photoluminescence spectral line shape of monolayer WS<sub>2</sub>,” *Curr. Appl. Phys.*, vol. 18, no. 8, pp. 941–945, Aug. 2018, doi: 10.1016/j.cap.2018.05.007.
- [18] S. Pak *et al.*, “Strain-Mediated Interlayer Coupling Effects on the Excitonic Behaviors in an Epitaxially Grown MoS<sub>2</sub>/WS<sub>2</sub> van der Waals Heterobilayer,” *Nano Lett.*, vol. 17, no. 9, pp. 5634–5640, Sep. 2017, doi: 10.1021/acs.nanolett.7b02513.
- [19] T. Han *et al.*, “Probing the Optical Properties of MoS<sub>2</sub> on SiO<sub>2</sub>/Si and Sapphire Substrates,” *Nanomaterials*, vol. 9, no. 5, Art. no. 5, May 2019, doi: 10.3390/nano9050740.
- [20] J.-M. Costantini, Y. Watanabe, K. Yasuda, and M. Fasoli, “Cathodo-luminescence of color centers induced in sapphire and yttria-stabilized zirconia by high-energy electrons,” *J. Appl. Phys.*, vol. 121, no. 15, p. 153101, Apr. 2017, doi: 10.1063/1.4980111.
- [21] G. Plechinger *et al.*, “Trion fine structure and coupled spin–valley dynamics in monolayer tungsten disulfide,” *Nat. Commun.*, vol. 7, no. 1, Art. no. 1, Sep. 2016, doi: 10.1038/ncomms12715.
- [22] A. Splendiani *et al.*, “Emerging Photoluminescence in Monolayer MoS<sub>2</sub>,” *Nano Lett.*, vol. 10, no. 4, pp. 1271–1275, Apr. 2010, doi: 10.1021/nl903868w.
- [23] Z. Sun and M. C. Gupta, “Laser annealing of silicon surface defects for photovoltaic applications,” *Surf. Sci.*, vol. 652, pp. 344–349, Oct. 2016, doi: 10.1016/j.susc.2016.03.028.
- [24] H. Nan *et al.*, “Strong Photoluminescence Enhancement of MoS<sub>2</sub> through Defect Engineering and Oxygen Bonding,” *ACS Nano*, vol. 8, no. 6, pp. 5738–5745, Jun. 2014, doi: 10.1021/nn500532f.

